Reference:
Proc.Intl.Soc.Opt.Eng.(SPIE), Vol. 5994, Chemical and Biological Sensors for Industrial and Environmental Security, ed. A.J. Sedlacek, S.Christesen, 58840J1-12, Oct. 2005

Status of Miniature Integrated UV Resonance Fluorescence and Raman Sensors for Detection and Identification of Biochemical Warfare Agents

William F. Hug[*a], Rohit Bhartia[b], Alexandre Taspin[b],
Arthur Lane[b], Pamela Conrad[b], Kripa Sijapati[a], RayD. Reid[a],
[a]Photon Systems, Inc., 1512 Industrial Park St., Covina, CA 91722
[b]Jet Propulsion Laboratory, Caltech, 4800 Oak Grove Dr., Pasadena, CA 91109

Abstract

Laser induced native fluorescence (LINF) is the most sensitive method of detection of biological material including microorganisms, virus', and cellular residues. LINF is also a sensitive method of detection for many non-biological materials as well. The sensitivity and specificity with which these materials can be classified depends on the excitation wavelength and the number and location of observation wavelengths. Higher levels of specificity can be obtained using Raman spectroscopy but a much lower levels of sensitivity. Raman spectroscopy has traditionally been employed in the IR to avoid fluorescence. Fluorescence rarely occurs at wavelength below about 260nm. Therefore, when excitation occurs at a wavelength below 250nm, no fluorescence background occurs within the Raman fingerprint region for biological materials. When excitation occurs within electronic resonance bands of the biological target materials, Raman signal enhancement over one million typically occurs. Raman sensitivity within several hundred times fluorescence are possible in the deep UV where most biological materials have strong absorption. Since the Raman and fluorescence emissions occur at different wavelength, both spectra can be observed simultaneously, thereby providing a sensor with unique sensitivity and specificity capability.

We will present data on our integrated, deep ultraviolet, LINF/Raman instruments that are being developed for several applications including life detection on Mars as well as biochemical warfare agents on Earth. We will demonstrate the ability to discriminate organic materials based on LINF alone. Together with UV resonance Raman, higher levels of specificity will be demonstrated. In addition, these instruments are being developed as on-line chemical sensors for industrial and municipal waste streams and product quality applications.

Keywords: native fluorescence, resonance Raman, biological detection

1. INTRODUCTION

Many types of instruments are available for testing biological or chemical materials if the quantities are plentiful and if sample handling, preparation, and use of reagents are possible and the size, weight, power consumption and cost of the instrument is not of concern. Our goal is development of miniature, hand-held, battery powered, instruments for first responder applications to detect and identify trace levels of biochemical agent contaminants in water and on surfaces. Employing an integrated combination of laser induced native fluorescence and Raman spectroscopic methods the instruments require no consumables or sample handling, and are non-contact and non-destructive to the samples or their substrates. Laser induced *native* fluorescence (LINF) is differentiated from traditional laser induced fluorescence (LIF) since it employs stimulation of fluorophors which are endogenous or native to the biological or chemical targets of interest and do not require derivatization with dye tags or other sample preparation or handling. The instruments have very high sensitivity and low false alarm rates in identifying threat particles or chemicals against a broad range of backgrounds.

When searching for trace levels of organic or biogenic materials, as required for hazardous biochemical agent detectors, an *in situ* instrumental methodology is needed that includes a high sensitivity *trigger phase* that can process relatively large amounts of sample material quickly, followed by a high specificity *confirmation phase* capable of obtaining detailed compositional information about samples identified as possible hazardous materials during the trigger phase. In the trigger phase it is sufficient to eliminate those particles or materials that are clearly non-organic or non-biogenic from those materials that are biological in nature including intact organisms, residues from organisms, virus', or other potentially harmful materials. Sensitivity is more important than specificity in this phase of detection. In the

confirmation phase it is important to give high levels of specificity in identification of the organic or biogenic material. More than one level of triage of a sample may be desired or required in order to formulate a response to an event. Confirmation sensors may take the form of a series of increasingly specific sensors, each of which provides more detailed information about a threat.

2. INTEGRATION OF UV RAMAN AND NATIVE FLUORESCENCE

2.1 Raman Scattering

Raman spectroscopy offers a non-contact method of extracting information on molecular structure and dynamics that does not suffer from many of the problem with infrared or near-infrared absorption spectroscopy, especially with measurements in aqueous solutions. In addition, Raman spectra can be obtained without "looking" through the sample. So the sample can remain in its natural, unperturbed, location. The number of vibrational or rotational modes or resonance frequencies of a molecule is given as 3N-6 (3N-5 for linear molecules), where N is the number of atoms in the molecule[i]. For simple, linear, diatomic molecules, there is only a single mode or resonance. Examples are H_2 where the resonance occurs at 4159 cm^{-1}, N_2 at 2331 cm^{-1}, and O_2 at 1556 cm^{-1}. Complex molecules, including biological macromolecules, can have very large numbers of atoms and can have subsequently very complex spectra.

Raman spectroscopy can be employed at a wide range of excitation wavelengths from the deep UV to the near infrared. Generally, dispersive Raman spectroscopy does not use excitation wavelengths above 790nm since the normal Raman shift range of interest (to about 4000 cm^{-1}) would extend beyond the spectral sensitivity range of typical silicon-based CCD array and may other types of common detectors. Normal Raman spectroscopy is a very inefficient process, with scatter cross-sections for typical "strong" Raman scattering bands in the range of 10^{-30} cm^2/molecule/steradian. To put this in perspective, in order to collect one Raman scattered photon/sec from a sample with 10^6 molecules within the field of view of a 532nm laser using an optical system with a collection solid angle of one steradian would require an incident laser flux of 10^{24} photons/sec/cm^2. This corresponds to a laser output nearly $4x10^5 W/cm^2$ irradiating the sample for 1 second. When a laser is focused to a small spot of perhaps 30μm square, the required laser power is nearly 4W for one second to obtain one Raman scattered photon per second. Normal Raman spectroscopy is therefore conducted in the visible or near infrared using very powerful, high intensity lasers to provide sufficient excitation photon flux to generate a measurable number of scattered photons. Prior to the introduction of lasers, Raman spectroscopy was a curious phenomenon with little practical use.

Since the introduction of visible and, more recently, ultraviolet lasers and a variety of modern detectors, the usefulness of the process has dramatically increased and continues to increase. One technique that has made a dramatic impact on the use of Raman spectroscopy in the measurement of biological material has been the use of pre-resonance and resonance Raman spectroscopy. Pre-resonance Raman occurs as the excitation photon energy approaches the first electronic excited state of the molecule and the Raman scattering cross-section begins to increase above its normal value. When the excitation photon energy occurs within the molecular manifold of the first electronic excited state, Raman scattering cross-sections and resulting scattering efficiency can dramatically increase in a process called resonance Raman. Resonance Raman has been demonstrated to yield scatter cross-section and signal improvement up to 10^8 over normal Raman. Resonance enhancement occurs dominantly within the electronic manifold of the absorbing species, greatly simplifying the ability to interpret the Raman spectra. Pre-resonance and resonance Raman spectroscopy as well as surface enhanced Raman spectroscopy have enabled dramatic increases in scatter cross-sections to values approaching 10^{-22} cm^2/molecule/steradian, enabling dramatic reductions in the required laser power to values in the microwatt range. This is making Raman methods of increasing value for practical uses, such as biochemical agent detection and identification as well as a host of other government and industrial applications. Excitation in the UV additionally enhances Raman scattering with dependence proportional to the fourth power of frequency, ν^4.

2.2 Native Fluorescence

A challenging problem to the use of Raman spectroscopy has been the ubiquity of fluorescence, which can be emitted by the sample under investigation or by impurities or background materials within the field of view of the laser. Fluorescence is a much more efficient process than Raman and even weak fluorescence can be much stronger than Raman, overwhelming and masking the Raman emissions. Fluorescence is not a scattering process. Fluorescence emission spectra do not have the vibrational fine structure observed in Raman spectra. However, even with the broad spectral character of fluorescence, significant specificity is possible with fluorescence, as will be shown later. When a

molecule is irradiated at an excitation wavelength that lies within the absorption spectrum of a molecule, it will absorb the radiant energy and be activated from its ground state (S_0) to an excited singlet state (Sn), with the electron in the same spin as the ground state. The molecule can then relax back from the excited state to the ground state by giving up excitation energy either non-radiatively or radiatively, depending on the local environment. In a nonradiative transition, relaxation occurs by thermal generation. In a radiative transition, relaxation occurs via fluorescence at specific emission wavelengths.

Many molecules and most organic and biological molecules have fluorophors or electronic states corresponding to energy in the ultraviolet. Figure 1 shows an excitation-emission matrix (EEM) diagram of benzene over a range of excitation wavelengths from 200nm to 400nm and emission wavelengths from 200nm to 600nm. Shown are iso-intensity contours resulting from elastic scattering and fluorescence. This diagram illustrates several important features of the relationship between elastic and Raman scattering and fluorescence. The diagonal line in the diagram represents elastic scattering where the emission and excitation wavelengths are equal: $\lambda em = \lambda ex$. Fluorescence emission is always Stokes-shifted to longer wavelengths. The amount of Stokes shift varies from one compound to another and as a function of excitation wavelength. In 1984 S.Asher[ii] showed that that no fluorescence is observable below 260nm for any sample, even with excitation at wavelengths as low as 220nm. This is also illustrated in Figure 1, where a fluorescence-free region is shown for excitation wavelengths below about 250nm and extending down to 200nm and below. Asher's explanation was that the smallest conjugated polyene or aromatic molecule to show significant fluorescence from its first excited state is benzene, which shows fluorescence only at wavelengths longer than 260nm. Larger aromatics show absorption bands below 260nm but excitation into these bands results in fast internal conversion of this energy into the lowest energy singlet or triplet excited state, and fluorescence or phosphorescence occurs at much longer wavelengths. As illustrated in Fig 1, shorter excitation wavelengths provide a wider range of fluorescence-free wavelengths in which to observe weak Raman scattering emissions without interference from fluorescence. At wavelengths below about 240nm, Raman scattering up to about 4000 cm^{-1} can be observed without interference from fluorescence. Figure 2 also clearly illustrates the fact that the fluorescence efficiency and Stokes shift is strongly dependent on excitation wavelength. At excitation wavelengths below about 220nm benzene shows little or no fluorescence at any wavelength. In this region, measurements can be made in full daylight conditions since the detection region is solar blind. S. Asher's 1984 paper opened up the field of ultraviolet resonance Raman spectroscopy, which is especially valuable for the elucidation of biological materials.

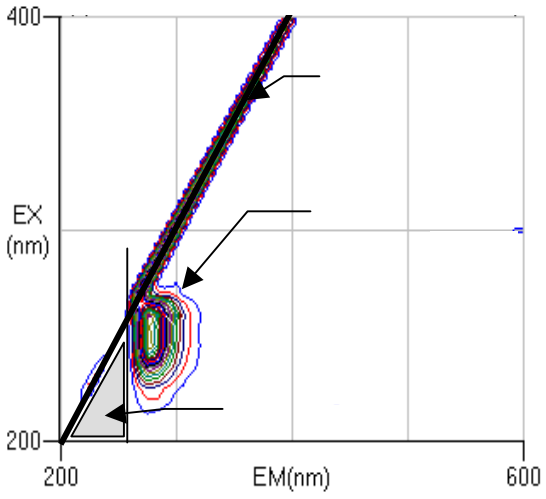

Figure 1. Excitation-Emission-Matrix diagram

When excitation wavelength is increased above about 240nm, fluorescence begins to interfere with Raman emissions occurring at larger Raman Stokes shifts. At excitation wavelengths above 260nm, fluorescence emissions will always overwhelm weak Raman emissions, even at small Raman Stokes shifts. A wide range of material fluoresces between about 260nm and 750nm, severely restricting the variety of samples for which Raman spectra can be obtained without fluorescence interference. For this reason, Raman spectroscopy is commonly performed in the near infrared or ultraviolet to avoid fluorescence interference.

3. SENSITIVITY AND SPECIFICITY OF NATIVE FLUORESCENCE DETECTION

All microorganisms require continual input of free energy through cellular metabolism. The source of this energy input is electrochemical potential between electron donors and acceptors. The primary carrier of free energy is adenosine triphosphate (ATP), which is derived from the oxidation of fuel molecules such as carbohydrates and fatty acids. Typical molecules responsible for the transport of energy within cells are porphyrins, quinones, flavins, NADH, etc. Other essential building blocks of living organisms are nucleic acids, amino acids and peptides, sugars and lipids, and polysaccharides. Amino acids are the most common chemical group in biological materials, characterized by an amino

group (NH_2) and a carboxyl group (COOH) and link to each other to form peptides and proteins. Phenylalanine, tyrosine, and tryptophan all have aromatic side chains with one or more benzene or phenyl rings. The aromatic side chains cause ultraviolet absorbance and fluorescence properties. When excited at an appropriate wavelength, these materials will provide a signature that can give a good indication of the general class to which the microorganism or organic material belongs. Many other organic and inorganic materials also fluoresce that are not harmful to humans. However, when the excitation and emission wavebands are carefully chosen, these can be discriminated against with high reliability.

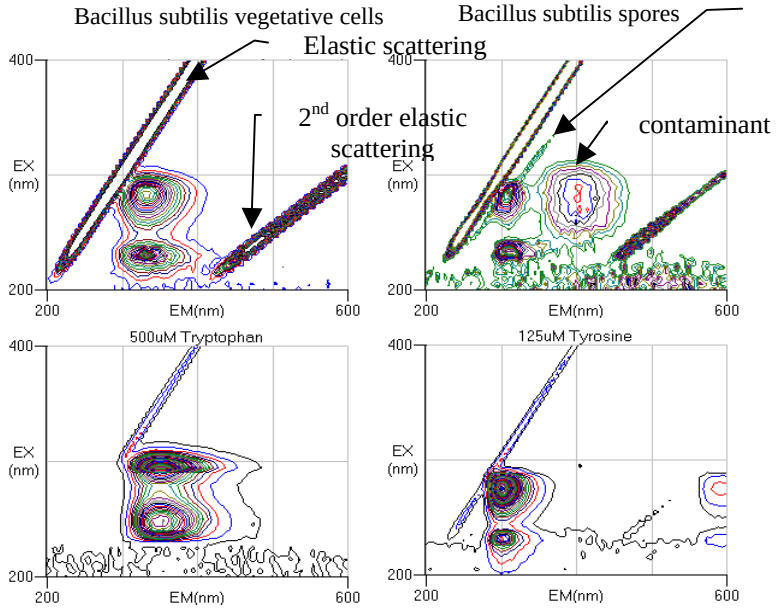

Figure 2. EEM diagrams of biological material

Figure 2 shows excitation-emission matrix (EEM) diagrams over a range of excitation wavelengths from 200nm to 400nm and emission wavelengths from 200nm to 600nm of four materials: Bacillus subtilis cells in the vegetative and spore form and tryptophane and tyrosine. The double fluorophors are a characteristic of the fingerprint of these materials, which have excitation maxima near 230nm and 280nm. Below about 270nm there is a fluorescence-free region between the elastic scattering line and the region of fluorescence of tyrosine. Resonance fluorescence of biological agents is likely the only technique sufficiently sensitive to discover, *in situ* without any sample preparation, the presence and rough classification of a single or few numbers of microorganisms. It is the only viable method of performing non-contact biological classification of aerosols in situ[iii] because of the small dwell time for observation in an aerosol stream. It is important to note that both the spores the vegetative cells have two optimum excitation wavelengths, one near 230nm and one near 280nm. Emission maxima vegetative cells at both excitation wavelengths are the same, at about 330nm, as expected. The EEM diagram for Bacillus subtilis in spore form (@10^4 per ml) is also shown in figure 2. Optimum excitation wavelengths will be described later. However, the optimum emission wavelength for spores is close to 305nm compared to 340nm for vegetative cells. This is a clearly distinguishable marker feature of spores. The data in Figure 2 were obtained in water and it known that there are some difference between organisms in a wet versus dry condition. However, the relative response is illustrated in this figure.

Driks[iv] shows that the spore coat for B. subtilis is dominated by tyrosine, whose fluorescence signature peaks near 300nm rather than the tryptophan, whose peak is near 350nm. This is shown by comparison with the TRP and TYR EEM diagrams shown below the B. subtilis in Fig. 2 above. A secondary optima occurring at Ex=280nm and EM=400nm is a result of a denatured alcohol contaminant in the sample. From the above EEM diagrams it is evident that B.subtilis vegetative cell fluorescence occurs at shorter wavelengths than pure Trp and long wavelengths than pure Tyr. The spore form is very closely related to Tyr as described by Driks.

It is a common notion that excitation at shorter wavelengths causes more interference with background materials. This is incorrect since each material has a unique fingerprint with the fluorescence cross-section and subsequent emission intensity dependent on both excitation and emission wavelength, as illustrated in figures 1 and 2 above, and 3 below. EEM diagrams in Fig. 3 below further illustrate the broad variation of fluorescence fingerprints of many common background materials. Fluorescence of most materials normally occurs between about 270nm and 700nm. Fluorescence at the shorter end of this wavelength range results from molecules that have single phenyl rings while fluorescence at the longer end results from molecules that have several phenyl or benzene rings, such as polyaromatic hydrocarbons. Most fluorescent materials exhibit one to three fluorescence peaks. Paper has strong peaks in the blue/green due to doping of paper with fluorescent dyes to enhance “whiteness”. Minerals typically have only one.

It is of interest to understand the ability to differentiate materials based on fluorescence alone. Later, in combination with elastic scattering for particle size determination, biological particles can be further differentiated. Target materials can include spores, vegetative cells, or biological residue materials such as aromatic amino acids, peptides or proteins, or nucleic acids, virus', etc. Background materials can include polyaromatic amino acids (PAH's), minerals, etc. The EEM fingerprint of most background materials is significantly different from a biological cell in either the spore or vegetative form. But even when a signature is similar, it is rarely similar enough that it cannot be differentiated, depending on the resolution of the spectrum obtained.

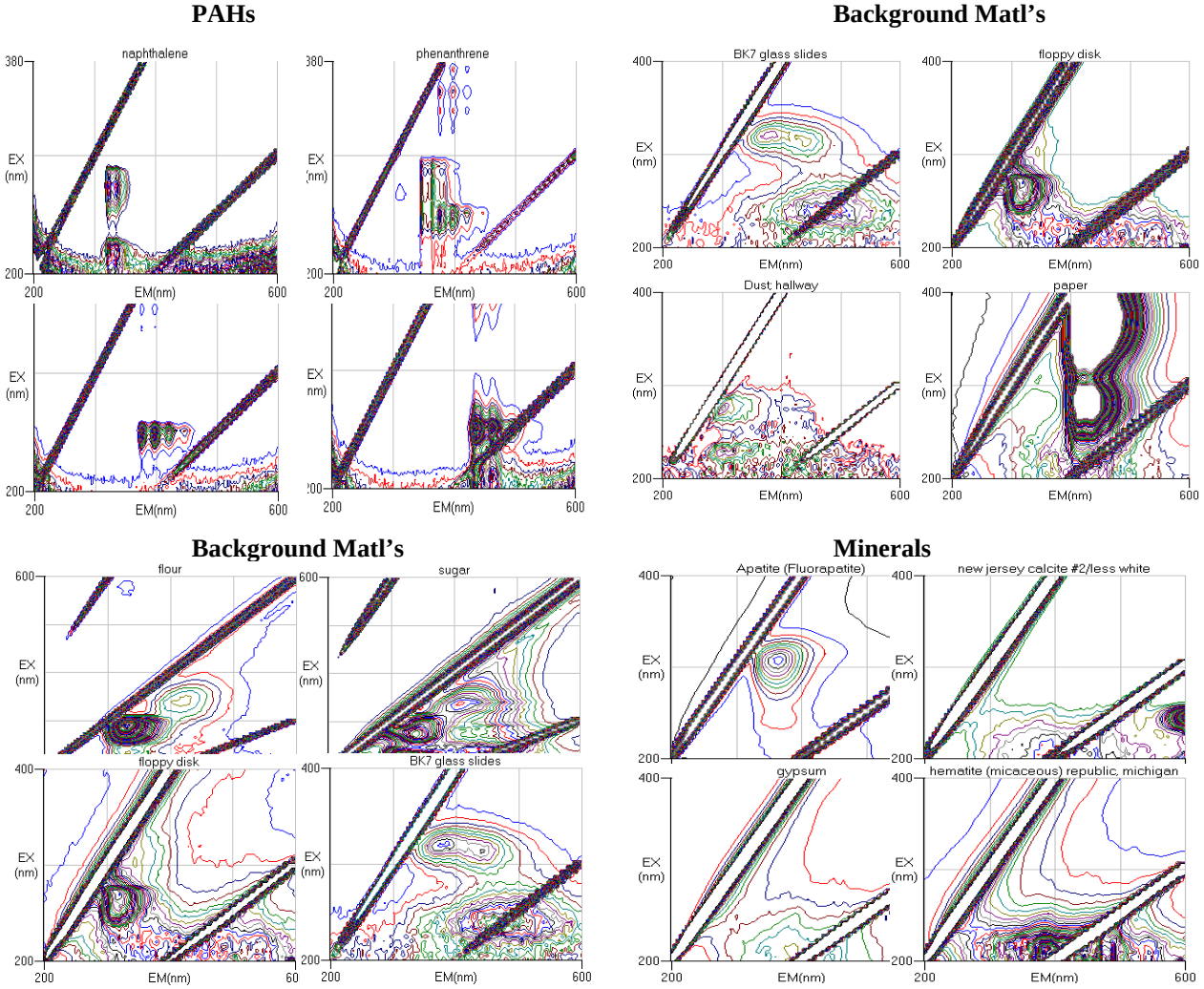

Figure 3. EEM diagrams of background materials

Figure 4, illustrates the ability to differentiate ten (10) groups (A through I) of pure samples excited at 235nm. Each group is made up of similar component materials which include organic and biological materials but which could also include minerals and other materials. High-resolution excitation-emission matrix (EEM) data sets of 61 pure samples were obtained using a Hitachi F4500 spectrofluorimeter where excitation ranged from 200nm to 400nm and emission ranged from 200nm to 600nm. Examples of these data sets are shown in Figs. 1, 2, and 4 above. At selected excitation wavelengths the relationship between the native fluorescence spectra of each material sample was compared using principal component analysis (PCA), although other analysis methods are also being investigated.

Samples illustrated in Figure 5 are grouped according to their general composition as illustrated in Table I. Table I is a list of the 61 samples and how they were grouped. Group A materials represent variants on single phenyl ring materials and are divided into two subgroups: 1 ring with 1-2 methyl group and phenylalanine and 1 ring with electronegative groups and tyrosine. Group B materials are bacterial spores of a variety of types. Group C materials are bacterial cells as well as lysates (supernatant and membrane fractions). Group D materials are two ring materials with or without R groups. Group E are indoles including tryptophan. Group F materials are 3 ring materials with bent conformation such as phenanthrene. Group G include folded 4 ring and straight 3 ring materials such as pyrene. Group H includes 5 ring and larger ringed organics such as perylene, NADH, etc. Group I materials are common household materials and pollens.

Table I. Samples compared: 61 samples in 10 groups according to basic composition

A. One ring compounds (black spheres) **A1. 1-2 methyl groups incl. Phe** phenylalanine-1Equal in nanopure1-1 b contains phenylalanine Gly phe ala Gly phe ser xylenes-1 **A2. Electronegative groups incl. Tyr** Tyrosine (dil1)-1Carpetaid-1ß contains benzene compounds toluene-1 dichlorobenzene-1 Glu tyr glu Gly tyr gly Leu tyr leu Lys tyr lys Nicety tyr eth ester **B. Spores (gray diamonds)** b atropheus-8b pumilis-8C. sporogen -8 (strain 1)C. sporogen -8 (strain 2)G. stearothermophil-8 **C. Whole cells and fractions (grey spheres)** 119 membrane,anaerobic 119 supernatent, “ 120 membrane, “ 120 supernatent, “ b.pumilus membrane, aerobically grown b.pumilus supernatant, “ b.pumilus whole cells, “ b.atropheus membrane, “ b.atropheus supernatant, “ b.atropheus whole cells, “ MR1 whole cells, “	**D. 2 ring compounds (open spheres)** 1,2 dimethnaph-21,3 dimethnaph-21,4 dimethnaphthalen-21ethyl naphthal-2acenaphthene-2dibenzothiophene-2 **E. Indole containing compounds (crosses)** carbazole-6 Indole-6tryptophan-6 **F. 3 ring compounds (bent) (open cubes)** 10 phenanthroline-3 'phenanthrene-3 **G. 4 ring (compact) and 3 ring (straight) (grey cubes)** 1 methylanthracene1-71methylpyrene-7pyrene-7anthracene3-7 **H. 5 rings(folded), 4 ring (straight), complex organics (small open cubes)** fluranthene-5 NADH-5perylene-5riboflavin-5 **I. Contaminants (black diamonds)**pink hibiscus pollen-0marigold pollen-0yellow hibiscus pollen-0 mech pencil lead-0 drywall-0corn starch (lush)-0 crayola chalk-0 ceiling tile-0 sweetnlow-0 splenda-0

Figure 5 clearly illustrates that microbial spores and vegetative cells are clearly differentiable from each other as well as all of the other chemical groups. The spore group was made up of a variety of spores which all clustered together. Whole vegetative cells and cell fractions from a variety of cell types also clustered together in a distinct group.

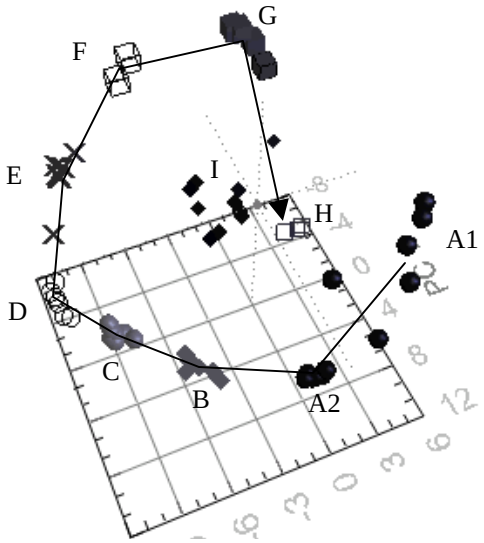

Figure 5. Full spectrum PCA positions of 61 samples in 10 groups. 235nm Excitation.

To quantify the ability to differentiate these materials the 3D PCA centroid and spherical standard deviation of each group was determined. Using a spherical standard deviation should be very conservative since all materials except household contaminants lie close to a line and are not distributed in a spherically symmetric cluster. In the following figures we define the ability to differentiate materials by two methods:

- Overall differentiability factor, OD_f, is the distance between the centroids of the two closest of the 10 groups, minus the sum of the standard deviations of the two closest groups.
- Spore differentiability factor, SD_f, is the distance between the spore group centroid and any other material, minus the standard deviation of the spore group.

The ability to differentiate between groups or individual materials is dependent on several factors including excitation wavelength, spectral resolution, and the number, bandwidth, and location of detection wavebands in sensors employing non-contiguous detection wavebands. Figure 6a shows the overall ability to differentiate all 10 groups, OD_f, identified in Table I as a function of wavelength for three confidence levels, corresponding to 1, 1.645, and 1.96 standard deviations of the group size. The optimum excitation wavelength for differentiating the groups of material selected is near 235nm. However, the shape and absolute values of OD_f with wavelength depends on the set of materials chosen for differentiation as well as the method of grouping materials. As an example, if spores or biological materials were not included, the resulting OD_f spectral distribution would be different. If a set of target and background materials were chosen which represented a specific situation in an industrial or municipal waste stream, in an ocean farming operation, or in a product or chemical factory, the choice of optimum excitation wavelength would be different. Optimum excitation wavelength is based on the choice of materials and groupings. For the materials and groups in Table I, 235nm is the optimum excitation wavelength.

The Spore Differentiability Factor, SD_f, is defined differently than OD_f and results in a slightly different curve, as shown in Figure 6b. The Spore Differentiability Factor, SD_f, is defined as the distance from the outer edge of the spore group to the nearest other chemical, since for this case all other chemicals are considered background chemicals and need not be grouped. The outer edge of the spore group is the centroid minus the spherical standard deviation of the group. SD_f is not as sensitive as OD_f to excitation wavelength below 235nm.

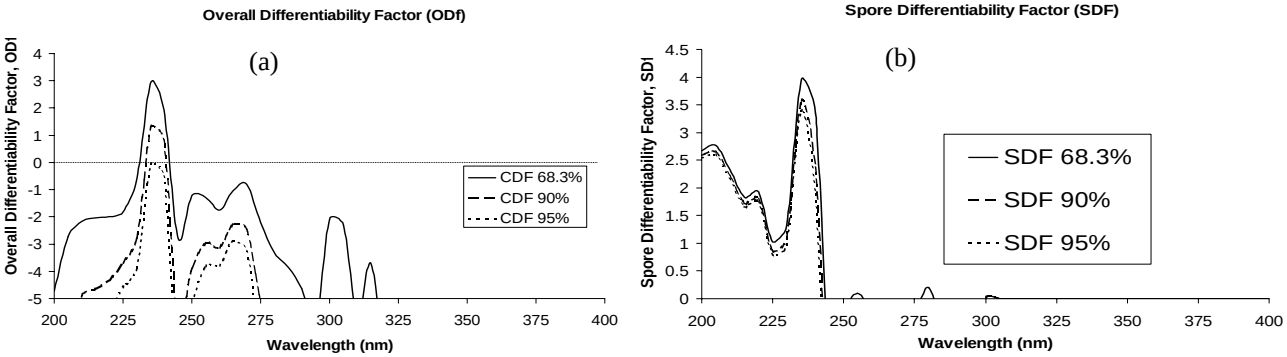

Figure 6. Overall Differentiability Factor, OD_f,(a) and Spore Differentiability Factor, SD_f (b) for 10 groups of samples

Figure 7 provides a more graphical representation of the wavelength dependence of the Spore Differentiability Factor where PCA diagrams for excitation at 235nm and 280nm show how the spore group merges with other groups of materials as the wavelength is increased from 235nm to 280nm. The PCA diagram for an excitation wavelength of 370nm shows most of the material samples merging into the origin (PCA = 0,0,0) since most materials offer little fluorescence signature when excited at 370nm, and not much differentiation is possible. Therefore this figure is not shown.

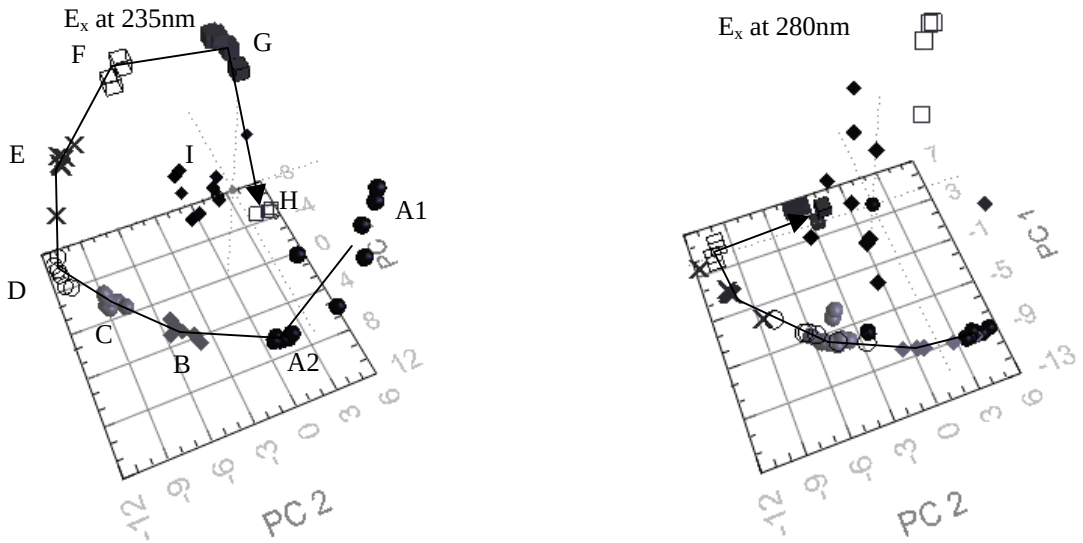

Figure 7. Comparison of PCA diagrams for 10 groups excited at 235nm versus 280nm, illustrating the merging of groups at non-optimum excitation wavelengths.

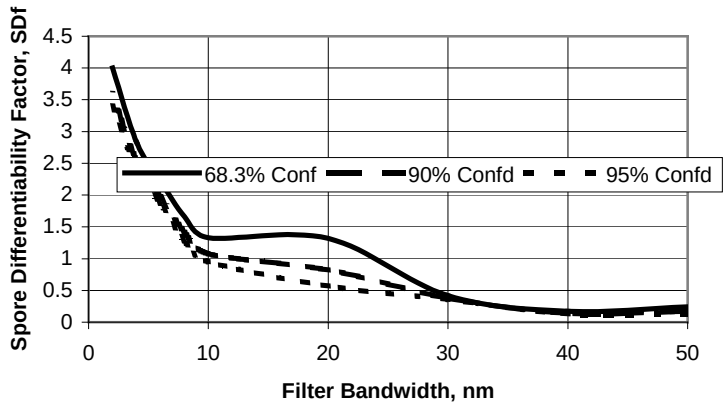

Figure 8. Spore differentiability factor versus spectra resolution

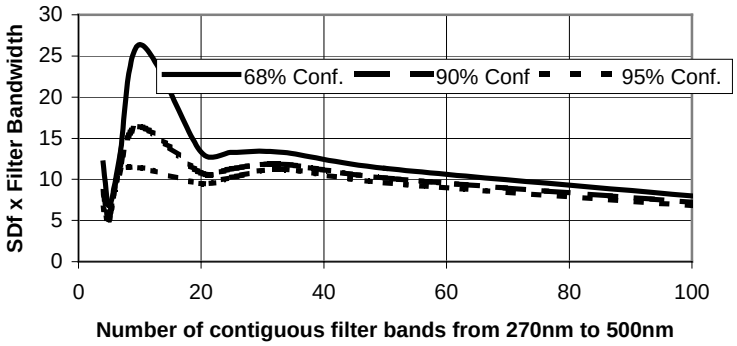

Figure 9. Product of differentiability and sensitivity, SD_fxfilter bandwidth.

The above data are based on data with a spectral resolution of 2nm. Spore differentiability is dependent on the spectra resolution at which the spectra are being compared, as shown in Fig. 8. Fig. 8 illustrates that spores can be differentiated with significant fidelity using low spectral resolution. Since the sensitivity of detection is proportional to the bandwidth of each detection band, lower spectral resolution also improves sensitivity. Optimizing the ability to detect and identify spores depends on the product of the spore differentiability factor and bandwidth, which is shown in Fig. 9. Note that at a confidence level of 68% (one standard deviation), the optimum number of contiguous filter bands is 10, corresponding to a filter bandwidth of 20nm. It is emphasized that these are contiguous detection bands. Significantly better differentiability can be achieved with fewer numbers of detection bands if the bands are non-contiguous and are located to optimize the targeted group of materials, which in this case are spores. Rather than 10 bands, it is possible to achieve the same differentiability with 5 or 6 bands, with concentration of the band centers located in the deep UV between 270nm and 350nm.

4. SENSITIVITY AND SPECIFICITY OF RESONANCE RAMAN DETECTION

Although Raman spectroscopy offers the ability to obtain higher specificity in identifying unknown materials, the sensitivity is much lower than native fluorescence. Table II below shows the cross-sections for fluorescence and Raman scattering for several nucleic and aromatic amino acids as well as whole cells with excitation in the deep UV.

The limit of detection (LOD) for either fluorescence or Raman emission is related to the number of photons collected in an optical system, $P_c = P_o\sigma\rho d^2/16f^2$, where P_c is the number of photons collected by the detection (objective) lens, P_o is the number of excitation photons delivered by the laser beam onto the sample, σ is the fluorescence or Raman scatter cross-section of the molecule or particle of interest (cm^2/mol) within a specific line or over a defined spectral bandwidth, ρ is the arial density of molecules or particles of interest (mol/cm^2), d is the diameter of the detection (objective lens) aperture and f is the distance of the sample from the detection aperture. Below in Table I are listed the fluorescence cross-sections of a whole B. subtilis spore and a single tryptophan molecule, both measured per nm of bandwidth at the peak of fluorescence emission at 330nm.

Table II. Native fluorescence and Raman cross-sections for biological materials

Target	Detection Band	Comment	Cross-section
			cm2/sr/nm/particle
B.subtilis spore[1]	330 Fluor. band	whole spore at 228nm	6.00E-14
TRP molecule[1]	330 Fluor. band	single molecule	2.75E-21
Adenosine[2]	1336 cm^{-1} Ram.band	whole line at 251nm	3.04E-22
Guanosine[2]	1575 cm^{-1} Ram.band	whole line at 251nm	1.56E-22
Guanosine[2]	1485 cm^{-1} Ram.band	whole line at 251nm	3.30E-22
B.Subtilis(LagPhase)	1615 cm^{-1} Ram.band	whole line at 229nm	1.04E-16

Comparing the cross-sections of whole cells excited near 229nm, native fluorescence per nm of bandwidth is about 500 times greater than Raman scattering for the whole 1615 cm^{-1} tyrosine line. At this excitation wavelength the Tyr line is resonance enhanced by many orders of magnitude over what it would be if excited in the visible. Nevertheless, the cross-sections are much smaller. Considering that fluorescence is normally measured in bandwidth near 20nm or 30nm, native fluorescence is more typically 20,000 times more sensitive than resonance Raman. As a result, it is difficult to make Raman measurements rapidly. Raman measurements typically require dwell time of more than a minute or two, even employing resonance enhancement.

A summary of the major taxonomic marker bands of highly degenerate molecular subgroups occurring within microorganisms is shown below in Table II.

Table III Taxonomic Raman marker bands for biological materials

Material	Raman Band Locations
Tryptophan	753 879 **1011** 1353 **1555** 1615
Tyrosine	831 852 **1180** 1210 **1615**
Guanine	1320 1365 **1485** 1577 1603
Adenine	**1337** **1485** 1580
Cytosine	**1530**
Dipicolinic Acid	**1019** **1195** **1396** **1446**

Identification of biopolymers or organisms using UV Raman spectroscopy depends on the ability to produce interpretable, reproducible spectra. DNA and cell surface antigens are the most attractive targets as potential markers for cellular or bacterial identification. Identification of organisms using UV Raman spectroscopy has focused on the ratio of a few taxonomic marker bands[v]. These band markers are based on ratios of tryptophan and tyrosine and DNA base pairs that can be characteristic of an organism. Most biological materials have repeating functional groups that are highly degenerate[vi]. These include nucleic acid base pairs and aromatic amino acids. These repeating units have Raman spectra that are very similar to the spectra of the monomers upon which they are based. Nelson has shown that based on the ratio of a few marker bands, many characteristics of microorganisms can be identified. Gram polarity of an organism can be determined by the 1555/1615 cm^{-1} intensity ratio with high being negative and low being positive. Cellular form is determined by the 1019/1615 cm^{-1} intensity ratio where high identifies the spore form because of the high content of dipicolinic acid and low identifies the vegetative form. A more specific identity can be determined using the 1530/1485 cm^{-1} intensity ratio that Nelson has shown is proportional to the mole percentage of guanine and cytosine. From this concentration, the identity of microorganisms can be determined with relatively high accuracy.

5. STATUS OF DEEP UV SOURCES

Much of the data demonstrating laser induced native fluorescence and resonance Raman spectroscopy as a powerful, reagentless, method of detection and identification of biological and other materials was generated using frequency doubled argon and krypton lasers, fourth and fifth harmonic, Q-switched, diode pumped solid state lasers with and without frequency shifters. Most of these lasers are large and consume much power and are not suitable for miniature hand-held sensors. Light emitting diodes (LEDs) and laser diodes (LDs) have not yet achieved short enough wavelengths to be of much use for the approaches described above. New lasers are beginning to emerge, including hollow cathode lasers emitting at 224nm, 248nm, 260nm, and 270nm that have linewidth less than 0.1 cm^{-1}. The smallest of these lasers is less than 0.3 liters in volume and consume less than 5W. A commercial version of one of these lasers is shown in Fig. 10.

Figure 10. 224nm HeAg and 248nm NeCu laser

Semiconductor lasers offer the prospect of significant miniaturization of UVLINF and UVRRS based sensors. Vegard's law[vii], illustrated below in Figure 11, shows the relationship between aluminum mole fraction and emission wavelength for AlGaN semiconductor materials. Theoretically, the emission wavelength of AlGaN devices can be composition tuned to emit anywhere between the limits of pure AlN at a bandgap of 6.2eV, corresponding to an emission wavelength of 200nm and pure GaN at a bandgap of 3.4eV, corresponding to an emission wavelength of 360nm. In order to obtain emission at wavelengths below 250nm will require AlGaN material with greater than about 60% aluminum content.

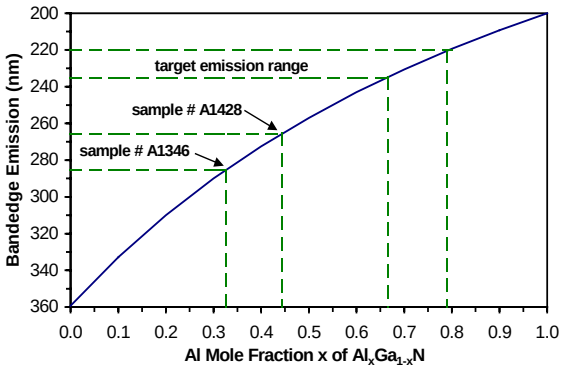

Figure 11. AlGaN semiconductor emission wavelength

Five major barriers have blocked the ability to produce semiconductor lasers that emit at deep UV wavelengths. These roadblocks are:

- Inability to p-dope high aluminum content AlGaN materials
- Inability to make ohmic contacts to high Al content AlGaN materials
- Inability to cleave facets of good quality in available substrate materials
- Lattice mismatch with available substrate materials resulting in high defect density in active region
- Difficulty in forming waveguiding layers in high Al content AlGaN

Because of one or more of these roadblocks, semiconductor lasers have been able to demonstrate emission only down to about 345nm. And, at this wavelength, the lifetime is presently very limited. Light emitting diodes have been demonstrated at wavelengths as low as 255nm.

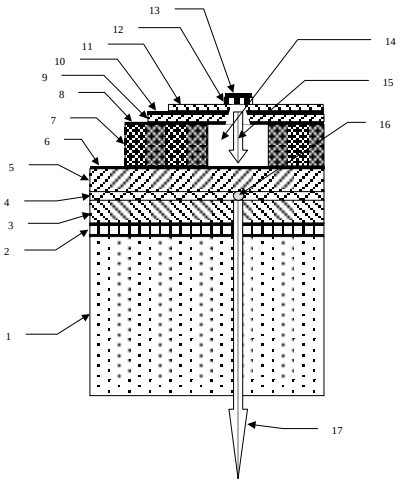

Figure 12. Schematic of ESUVOS

To avoid roadblocks associated with p-doping and ohmic contacts associated with pn-junction devices, our basic approach had been to use a ballistic electron beam to generate electron hole pairs in the active region of the AlGaN semiconductor material. We call this approach an Electron-beam-pumped Semiconductor UV Optical Source, or ESUVOS, as an extension of the DARPA-sponsored SUVOS program, and shown schematically below in Figure 12. In contrast to pn-junction (SUVOS) devices, each ballistic electron in an ESUVOS produces many hundreds of electron-hole pairs whereas only one pair is produced per electron in a pn-junction device. As a result, the devices will operate and approximately 500 times lower current and 500 times higher voltage that pn

junction devices. We believe this approach is a pragmatic solution that leapfrogs the most significant problems impeding the development of deep UV semiconductor lasers: p-doping and ohmic contact problems. This approach also allows us focus other important, but not as blocking, issues related to active region defects created by lattice mismatch, etc., facet quality, and waveguiding problems. If and when the problems of p-doping and ohmic contacts are solved for pn-junction AlGaN devices with Al-content above 60%, our approach will have enabled significant progress to be made on these other issues. Figure 13 is an example of an electron beam pumped light emitting triodes (ELETs) emitting at 240nm, which is suitable for optimum differentiation of biological particles. We have also demonstrated ELETs as low as 233nm. The device illustrated in Fig. 12 is about 1 mm^3 in size. It must be contained in a vacuum device of the order of 1 cm^3, similar to the device shown as an insert in Fig. 13.

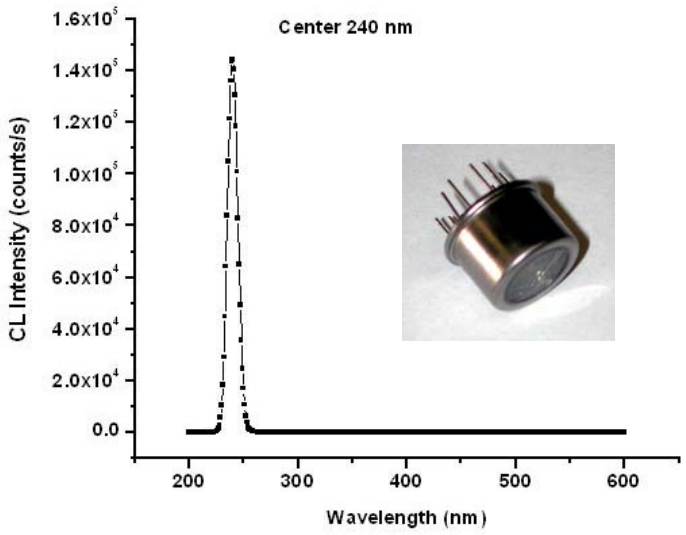

Figure 13. Emission spectra of ELET

6. STATUS OF HAND-HELD, REAGENTLESS, BIOCHEMICAL SENSORS

Photon Systems is developing hand-held, battery powered biochemical surface scanner devices to detect trace levels of biological and chemical contamination on a wide range of surfaces. Figure 14a shows an illustration of the ultimate device being developed. Figure 14b shows a breadboard device as it was deployed in Antarctica in February 2005.

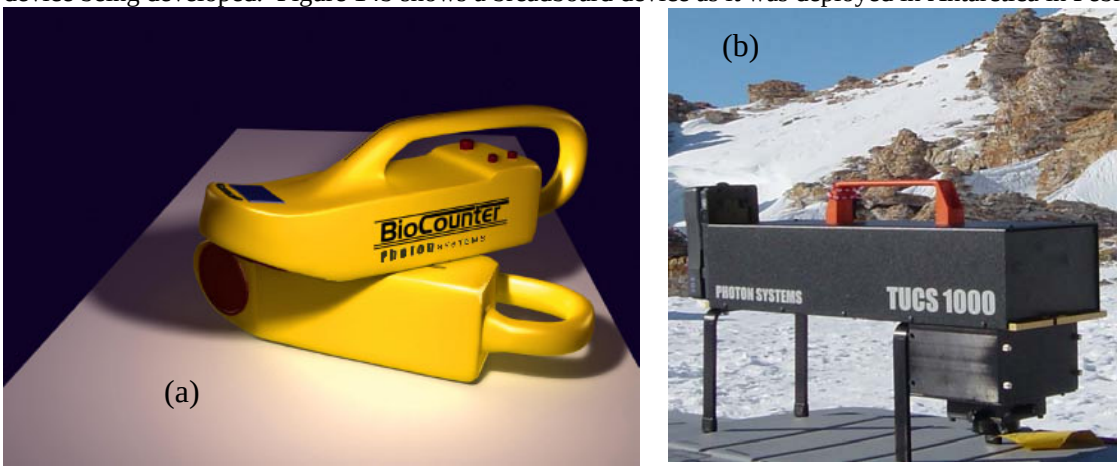

Figure 14. Hand-held, battery-powered, reagentless biochemical sensors based on UN LINF and UVRRS

Various versions of instruments similar to that shown in Fig. 14b have been built and deployed in the Artic, Antarctic and deep Ocean below 8000 feet in depth. Each of these instruments employed either at 224nm HeAg laser or 248nm NeCu laser in conjunction with multi-band native fluorescence and Raman sensors which were gated in synchronism with the laser to enable measurement of trace levels of contaminants, down to a single spore, on widely varying backgrounds. The miniaturized Instrument on a Chip (IOC) shown in Fig. 15, is a photomultiplier (PMT) controller and digital boxcar integrator and averager, not much larger than the quarter used for size reference. The IOC provides over 9 decades of detection sensitivity range, a 32 bit, 75 MIP microprocessor with 2M RAM and 256K flash memory, and enables digital integration over selected time intervals of the

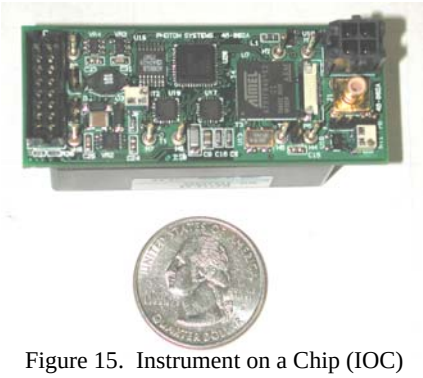

Figure 15. Instrument on a Chip (IOC)

native fluorescence or Raman emissions from a target. We have also developed an ultra-miniature Raman analyzer (UVRRA), shown below in Figure 16. The overall dimensions of the UVRRA is about 4 inches along the optical axis, about 0.75 inches thick and about 4 inches wide. This UVRRA consists of: an objective lens with 0.5 numerical aperture; an elastic scatter blocking edge filter with OD 6 at the laser excitation wavelength of 248.6nm at greater than 85% transmission above about 400 cm^{-1} of Raman shift; an angle tuning filter with 40% transmission with linewidth about 40 cm^{-1} and a tuning range from about 1000 cm^{-1} to 2200 cm^{-1}; a visible light blocking filter with blocking above 280nm over OD 6 and transmission below 280nm about 50%; a space qualified stepper motor with 10,000 steps per revolution corresponding to a step size about 5 cm^{-1}; a sealed, metal can, photomultiplier tube with deep UV photocathode with QE about 25% and integrated high voltage power supply; and a digital PMT controller with gated boxcar integrator and averager which allows optical gain selection over a six orders of magnitude and electronic gain over a three decade range. The detector and Raman shift selecting stepper motor are digitally controlled via a bi-directional RS488 interface. This instrument is capable of self-calibration against several standards.

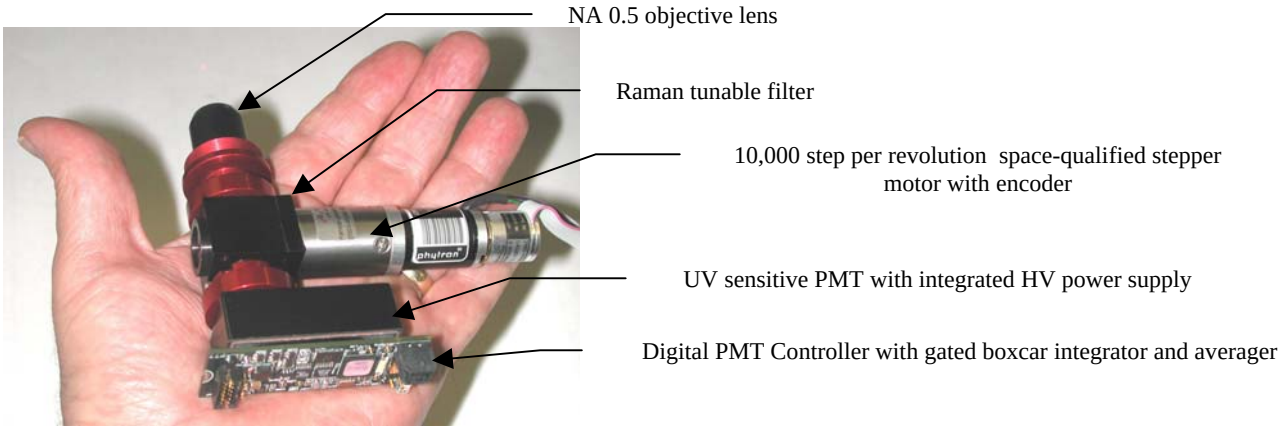

Figure 16. Photo of ultra-miniature UV resonance Raman confirmation sensor

7. CONCLUSIONS

Hand-held, battery powered, reagentless, biochemical agent detectors are emerging with the potential to detect trace levels of biological and chemical contaminants, down to the level of a single spore. Rugged and reliable breadboard sensors have already been developed and demonstrated in very harsh conditions from the Artic to the Antarctic to the deep Ocean. Other instruments based on an integrated combination of deep UV laser induced native fluorescence and resonance Raman spectroscopy are being developed for monitoring of water quality and contamination.

8. ACKNOWLEDGEMENTS

We would like to thank DARPA and NASA for their support of this work. We would also like to thank several people for their contributions, including: Ted Moustakas, Anirban Bhattacharyya, and Ramya Chandreskar of Boston University, Photonic Devices Center; and Chris Brown and Bill Nelson of University of Rhode Island.

REFERENCES

[i] N.B. Colthup, L.H.Daly, S.E. Wiberley, *Introduction to Infrared and Raman Spectroscopy* (Academic Press, 1990).
[ii] S.A.Asher, C.R. Johnson, *Raman Spectroscopy of a Coal Liquid Shows That Fluorescence Interference Is Minimized with Ultraviolet Excitation*, Science, 225, 311-313, 20 July 1984.
[iii] Faris, G.W., R.A. Copeland, K. Mortelmans, and B.V.Bronk, *Spectrally resolved absolute fluorescence cross sections for bacillus spores*, App.Opt.,Vol.36, No.4, pp.958-967, 1 February 1997.
[iv] Driks, A., *Bacillus subtilis spore coat*, Microbiology and Molecular Biology Reviews, Vol.63, No.1, pp.1-20, Mar. 1999.
[v] Nelson, W.H. , Manoharan, R., and Sperry, J.F. Appl. Spect. Rev. 27(1), 67, 1992
[vi] W.H. Nelson, R.R. Dasari, M. Feld and J.F. Sperry, *Intensities of Calcium Dipicolinate and Bacillus Subtilis Endospore Raman Spectra Excited with 244 nm Light*, (In press, Applied Spectroscopy)
[vii] L. Vegard, Z. Phys. **5**, 17 (1921); M.F. Thorpe and E.J. Garboczi, Phys. Rev. B **42**, 8405-8417 (1990).